Published in final edited form as:
J Comp Neurol. 2010 July 15; 518(14): 2693–2709. doi:10.1002/cne.22359.

Prefrontal Cortical Inputs to the Basal Amygdala Undergo Pruning During Late Adolescence in the Rat

Victoria L. Cressman[1,2], **Jordan Balaban**[2], **Sara Steinfeld**[2], **Alexei Shemyakin**[1], **Peter Graham**[2], **Nelly Parisot**[1], and **Holly Moore**[1,2,*]

[1]Department of Psychiatry, College of Physicians and Surgeons, Columbia University, New York, New York 10032

[2]Division of Integrative Neuroscience, New York State Psychiatric Institute, New York, New York 10032

Abstract

Transformations in affective and social behaviors, many of which involve amygdalar circuits, are hallmarks of adolescence in many mammalian species. In this study, using the rat as a model, we provide the first evidence that afferents of the basal amygdala (BA) undergo significant structural remodeling during adolescence. We used quantitative tract-tracing and gene expression profiling methods to characterize changes in the medial prefrontal cortical (mPFC) inputs to the BA across ages analogous to the late juvenile period [postnatal day (P) 25], late adolescence (P45), and adulthood (P90) in the rat. As assessed after deposition of Fluorogold into the BA, the number of BA-projecting neurons in the mPFC remained stable between P25 and P45 but decreased by about 50% between P45 and P90. Anterograde tract tracing with biotin dextran amine deposits centered in the ventral prelimbic cortex revealed that, during this period, the density of mPFC-derived axon terminals in the BA also decrease significantly, an effect particularly evident in the dorsal basolateral nucleus. Within the BA, there were also highly significant changes in gene expression indicative of neurite or synaptic plasticity, most notably in the Ras/GTPase superfamily, and in pathways that regulate cytoskeletal dynamics and steroid synthesis/lipid metabolism. These data provide convergent evidence that mPFC inputs to the BA are pruned during late adolescence or early adulthood. Moreover, the structural remodeling within these afferents may be accompanied by significant changes in neurite plasticity within the BA.

Keywords

amygdala; prefrontal cortex; axonal retraction; adolescence; Ras GTPase; gene expression profiling; anterograde; retrograde

Adolescence is a distinct stage in brain development marked by nonlinear changes in cognition, affective regulation, and behavior (Casey et al., 2008; Spear, 2000) and associated with a precipitous rise in the risk for psychiatric disorders, including schizophrenia, anxiety, substance abuse, and mood disorders (Kessler et al., 2005; Paus et al., 2008). It has been postulated that adolescent changes in the prefrontal cortex (PFC) and the amygdala are important for the maturation of cognitive regulation of affective behavior (Blakemore and Choudhury, 2006) and, if disrupted, can trigger the pathophysiology underlying several

*CORRESPONDENCE TO: 1051 Riverside Drive, Box 14, New York, NY 10032. hm2035@columbia.edu.

Additional Supporting Information may be found in the online version of this article.

psychiatric disorders (Paus et al., 2008). These hypotheses are supported by structural and functional evidence for adolescent-specific changes in the PFC and amygdala in many species (Amsel and Chen, 1976; Guyer et al., 2008; Hare et al., 2008; Koshibu et al., 2004; Monk et al., 2003; Rakic et al., 1994; Rubinow and Juraska, 2009; Van Eden and Uylings, 1985; Woo et al., 1997; Zehr et al., 2006) and abnormalities in these regions in psychiatric disorders emerging in adolescence and young adulthood (Aleman and Kahn, 2005; Casey et al., 2008; Phillips et al., 2003).

The studies cited above also highlight the possibility that connectivity between the PFC and the amygdala is not stable during adolescence. Consistent with this, Cunningham et al. (2002,2007) have shown that the density of amygdalar axonal fibers within the PFC continue to change through early adulthood in the rat. Studies in non-human primates have also provided evidence that PFC afferents and intrinsic circuits change during adolescence (Elston et al., 2009;Lewis et al., 2004). However, to date, only a handful of studies have examined changes in structural connectivity within the adolescent brain, with none examining medial (m)PFC efferents or amygdalar afferents. To address this, the present study was designed to characterize the adolescent development of the mPFC projections to the basal amygdala (BA; including basolateral and basomedial subnuclei), a key circuit in affective regulation (Blumberg et al., 2004;Drevets, 2003;McDonald et al., 1999;Vertes, 2004). We focused on axonal remodeling, a process critical for neural circuit maturation (Clarke and Innocenti, 1986;Luo and O'Leary, 2005;Schreyer and Jones, 1988;Tessier-Lavigne and Goodman, 1996) that has been well characterized in the early postnatal brain but minimally studied in the adolescent brain (but see above; see also Bagri et al., 2003). Our experiments were conducted in the rat, a rodent that exhibits physiological and behavioral transitions characteristic of adolescence. These transitions begin at about postnatal day (P) 28 and continue through P45 (Andersen et al., 2002;Spear, 2000). In the present study, we combined retrograde and anterograde tract-tracing methods to quantify changes in the mPFC inputs to the BA during adolescence. We report that the mPFC projections to the BA, particularly the innervation of the dorsal basolateral nucleus, begins to decrease during or after late adolescence, reaching a level in adulthood that is approximately 50% of the level at early adolescence. Moreover, gene expression profiling coupled with functional pathway analyses revealed that, during this period in which mPFC inputs to the BA undergo pruning, there are functional changes within the BA in molecular pathways that regulate neurite plasticity.

MATERIALS AND METHODS

Subjects

The experiment was approved by and conducted in accordance with the policies of the Institutional Animal Care and Use Committees at the New York State Psychiatric Institute and Columbia University. Pregnant Wistar rats were purchased from Hilltop Laboratories (Scottdale, PA). Litters were culled to eight pups and weaned at P25. Only male offspring were used in these experiments. At weaning, male offspring were randomly assigned to each of the age groups used within an experiment and housed in pairs or triplets until used as described below.

Stereotaxic surgery and histology

Surgery—Under isoflurane anesthesia, the rat was mounted in the stereotaxic frame, and anesthesia, body temperature, and respiration rate were monitored. Tracer injections were made according to the methods described below. After surgery, once rats were ambulatory, they were placed back into their home cage (with one to two littermates) and monitored daily during the recovery period, which varied for each tracer (see below).

Fluorogold injection and tissue processing—Our goal was to capture the mPFC axonal fibers present in the BA at P25, P45, and P90; therefore, we made our retrograde injections at these time points. A 1% solution of Fluorogold (FG; Fluorochrome, Denver, CO) in sterile distilled water was iontophoretically injected unilaterally into the BA, defined here as encompassing the basolateral and the caudal portion of the posterior basomedial amygdalar nuclei of Paxinos and Watson (1998; for schematic of the BA see Fig. 1A,B). The coordinates (see Table 1) were adjusted through pilot experiments to reliably reproduce equivalently sized deposits in the BA across all three ages. FG was iontophoresed using a pulled glass pipette with a 50-μm tip and a constant current source set at +5 μA with 5 second on/off pulses for 20 minutes. The pipette was slowly removed 1 minute following the last pulse.

Using the above-described methods for tracer iontophoresis, we conducted two experiments, which differed in the survival period applied. In experiment 1, a 14-day survival period was used to ensure maximal transport of the tracer for a quantitative comparison of mPFC projections to the BA in animals injected at P25 or P90. In experiment 2, FG was iontophoresed into the BA at P25, P45, and P90, and brains were harvested after a 4-day survival period. This survival period was within the range recommended by the manufacturer (typical range 3–5 days; http://www.fluorochrome.com/FGProtocol.htm#MainProtocol) and allowed us to examine multiple points in adolescence (a 20-day span in the rat; Spear, 2000) to approximate the age at which pruning begins in the mPFC-BA projection.

At the end of each transport period, the rats were deeply anesthetized with sodium pentobarbital and perfused with cold isotonic saline and freshly prepared cold 4% paraformaldehyde in phosphate buffer. The brains were postfixed in 4% buffered paraformaldehyde overnight and then cryoprotected with ascending concentrations of sucrose in buffer. To partially meet the criterion of systematic random sampling for quantification of retrogradely labeled neurons (for review see Mouton, 2002; see below), the brains were sectioned as follows. A random starting point within 300 μm of the frontal pole was chosen, and then sections were collected systematically from that point to the posterior border of the hippocampus. For experiment 1, 40-μm-thick sections were collected every 160 μm (experiment 1) and thawmounted onto coated glass slides. In experiment 2, the methods were identical except that the section thickness and sectioning intervals were 30 and 300 μm, respectively. Mounted sections were dehydrated/defatted, coverslipped, and stored in the dark for subsequent analysis of FG by fluorescence microscopy. For each brain, a set of adjacent sections (cut with the same sectioning thickness and interval) was counterstained with a cell body stain and used for histological verification of the anatomical boundaries of the regions of interest (see below).

Biotin dextran amine injection and tissue processing—To examine more directly the local changes in mPFC afferents within the BA across adolescent development, we conducted anterograde tract-tracing experiments with biotin dextran amine (BDA; 10,000 MW; Invitrogen, Carlsbad, CA). Because our goal was to quantify the mPFC-derived axon terminals at the same ages used for the retrograde tracing studies (P25, P45, and P90), BDA was iontophoresed into the mPFC of P19, P39, and P84 rats to allow sufficient time (6 days) for tracer transport for the examination of fibers at P25, P45, and P90. Studies in rodents using BDA to examine relatively long corticosubcortical fiber tracts have typically used transport periods between 4 and 14 days. Through pilot studies, we determined that the fiber densities in the BA were similar following a 6- or 14-day transport period. For the injection, a pulled glass pipette with a 25-μm tip was filled with 10% BDA in isotonic saline (0.9%) and lowered into the mPFC. BDA was iontophoresed using a constant current source set at +7 μA with 5-second on/off pulses for 15 minutes. The stereotaxic coordinates targeted the

ventral prelimbic cortex. This was based on the robust retrograde labeling from the BA in this region, which was, in turn, consistent with published anterograde tracing studies showing projections from this region to the BA, particularly the basolateral nucleus (McDonald et al., 1996). To fill this subregion adequately, two injections separated by approximately 0.8 mm along the anterior-posterior axis were made at empirically-determined custom coordinates for each age group (Table 1). After a 6-day survival period, animals were perfused, and brains were postfixed and cryoprotected as described above. As with the retrograde study, the brains were sectioned systematically from a random starting point within 270 μm of the frontal pole to the posterior extent of the hippocampus. Free-floating sections 45 μm thick and separated by 135 μm were oxidized in buffered hydrogen peroxide, rinsed, and then incubated in an avidin-biotin complex solution for 1 hour (Vector Laboratories, Burlingame, CA). After rinsing, fibers were revealed with 0.02% diaminobenzidine, 0.3% ammonium nickel sulfate, and 0.01% hydrogen peroxide for 2 minutes and then rinsed, mounted, counterstained with neutral red, dehydrated/defatted, and coverslipped.

Quantification of retrograde and anterograde labeling

Identification of comparable tracer deposits between animals—Injection sites for both retrograde and anterograde studies were evaluated and compared according to location and size. To evaluate the location of the tracer deposit, photomicrographs of every coronal section collected from the amygdala and mPFC (for the retrograde and anterograde experiments, respectively) were taken, centering on the injection site. For each animal, an array of these photomicrographs was then assembled, standardizing the position of a photomicrograph in the array according to its distance from Bregma. Panels for all of the animals were then aligned and visually compared by two investigators, and brains containing tracer deposits in similar locations were identified. With this set of brains, both investigators independently evaluated and compared the gross size of the injection so that injections with similar locations but grossly different sizes were excluded. The volumes of the injection sites were then quantified as described below.

Evaluation of the injection site—The injection volumes for both the retrograde and the anterograde tracers were determined by drawing contours using a ×2.5 objective lens around the injection site in the amygdala and mPFC, respectively. Boundaries for the BA injection site were defined based on the homogeneity of the fluorescence, excluding regions containing discretely labeled cell bodies without additional background staining. For the mPFC, the BDA injection site contours were drawn around the regions containing the BDA-filled soma and where the neuropil that appeared to be continuous with (e.g., containing dendrites of) the filled cells. The neuropil included in the injection site contour was densely stained. Fibers of passage (e.g., in layer VI or white matter) were not included in the injection site. Representative examples of dye deposits and the contours used to define the injection sites are shown in Supporting Information Figure 1 (FG in the BA) and Supporting Information Figure 2 (BDA in the mPFC).

The volumes of tracer deposits and of the regions of interest (ROIs) were estimated using the Cavalieri estimation method. All stereological methods were adapted from Mouton (2002) and performed in Stereoinvestigator software (MicroBrightField, Williston, VT). Identification of injection sites and ROIs within each brain and initial quantification of neurons and fibers were first performed by one or two investigators with detailed knowledge of the anatomy of the prefrontal cortex and amygdala. This process was necessary to ensure anatomical homology of injection sites and ROIs across different-aged brains. Quantification of neurons or fibers within the ROIs was then verified by an observer blind to the age of the brain.

Neurons retrogradely labeled from the BA—The mPFC ROI was ipsilateral to the injection site and defined à priori based on previous reports describing projections from these regions to the BA (Cassell and Wright, 1986; Gabbott et al., 2005; McDonald et al., 1999; Pinto and Sesack, 2000; Sesack et al., 1989; Vertes, 2004). This ROI included the anterior cingulate (ACg), prelimbic (PL), infralimbic (IL), and dorsal peduncular (DP) regions, from the anterior border of the DP caudally to the anterior border of the genu of the corpus callosum [structural borders as defined by Paxinos and Watson (1998) and Paxinos (1995)]. The mPFC ROI is shown at representative coronal levels in Figure 1C.

To meet the criterion of systematic random sampling, the mPFC ROI was sampled in its entirety, the section interval having been set during sectioning (see above). Fluorescent neurons were visualized using a wide-band ultraviolet filter with a ×20 objective lens. To quantify the neurons within the ROI, a grid (150 μm × 150 μm) was superimposed on the contour in StereoInvestigator (MicroBrightField), and fluorescent neuronal cell bodies were marked in each grid square contained in the contour. Examples of the FG-filled mPFC neurons are shown in Supporting Information Figure 3. Neuroexplorer (MicroBrightField) was then used to calculate the number of markers within each contour. This number was summed across all sections containing the ROI. Using the adjacent cell-body-stained sections, the contours of the ROI in each section were redefined according to anatomical landmarks and cell architectonics described in the references cited above. This more precise contour was then aligned with the adjacent FG-only section, using fiduciaries such as prominent blood vessels and other landmarks visible on both sets of sections, and labeled cells within the Nissl-based contour were counted. To obtain the most accurate estimate of the frequency of labeled neurons within the ROI, it was necessary to count all labeled neurons within in the ROI. This resulted in a sampling of approximately 25% of the volume of the mPFC ROI in experiment 1 and 10% in experiment 2. The number of retrogradely labeled neurons counted was corrected for the volume (and number of sections) sampled, which, in turn, was consistent across age groups.

Fibers within the BA anterogradely labeled from the mPFC—The ROI for quantification of mPFC-derived axonal terminals in the BA included the basolateral amygdalar nucleus (anterior and ventral divisions) as well as the ventrally adjacent posterior basomedial amygdala (Paxinos and Watson, 1998; see Fig. 1B). Fibers were marked at ×40 magnification using a 70-μm counting frame, a 150 × 150 μm grid, and a cycloid width of 25 μm. The rotation angle of the grid was randomized for each section. Fiber density was determined using the L-cycloids method combined with the optical fractionator method to estimate the total fiber length and the fiber length per unit volume within the contour (Mouton, 2002).

Photomicrograph production—Images were captured as jpeg files in StereoInvestigator and opened in Adobe Photoshop if adjustments were needed in the contrast or sharpening (for high-magnification images). Images were then opened in Adobe Illustrator for figure layout. To display the axonal fibers better for publication, the contrast of photomicrographs in Figure 8C–H was increased, and a filter was used to sharpen the fibers. The high-magnification photomicrograph in Supporting Information Figure 3C was also sharpened for better clarity of the filled cells.

Statistical analysis for quantitative anatomical experiments

Tracer deposit volumes in each experiment, as well as the volumes of the mPFC and BA, were compared across age groups with either one-way ANOVAs (for three age groups) or Student's two-tailed *t*-tests. The effect of age on the density of retrogradely labeled neurons was analyzed with an ANOVA including tracer deposit volume as a covariate. A significant

omnibus F in experiment 2 was further analyzed by using the "repeated" contrast method in which the two allowable contrasts were "P25 vs. P45" and "P45 vs. P90." For the anterograde tracing experiment, the effect of age on fiber length per unit volume was assessed with the same statistical design as in retrograde experiment 2.

Comparison of gene expression patterns

Pregnant Wistar dams were obtained from Hilltop Laboratories (Scottdale, PA). Five litters were culled to eight pups per litter on P1 and weaned at P25. Animals were group housed until the time of euthanasia. Within each litter, one male was killed at P45 and one at P90. Animals were quickly sedated with isoflurane gas until reflexes were gone, and then decapitated to minimize gene expression changes induced by the sedation process. Brains were isolated, flash-frozen in cold isopentanes, and mounted on a cryostat. The BA of each hemisphere was harvested with 1-mm-diameter punches and immediately homogenized in Trizol (Invitrogen). RNA was then extracted with phenol-chloroform, precipitated by glycogen and isopropanol, and resuspended in RNAse-free water. cDNA generated from each RNA sample was then hybridized on a separate Affymetrix Rat Expression Array 230 2.0 (Affymetrix, Santa Clara, CA). Quality-control parameters for each of the array platforms were as follows: noise (raw Q) <5, scale factor <3, and background average <100. One P45 and one P90 case that met the noise but slightly exceeded the background threshold were also included. The robust multiarray average (RMA) algorithm was used for background adjustment and normalization.

In this study, we used both ErmineJ (Lee et al., 2005) and Ingenuity Pathway Analysis (IPA; Ingenuity Systems, www.ingenuity.com) to increase the possibility of finding functionally relevant changes and to cross-validate the results of each analysis. ErmineJ and IPA are independent programs that take a systems biology approach by identifying potential changes in biological functions within a gene expression data set. For the ErmineJ analysis (made available by Dr. Paul Pavlidis and colleagues at http://bioinformatics.ubc.ca/ermineJ/), the numbered probe sets and *P* values from the RMA analysis of the P45 and P90 amygdala arrays were entered and analyzed with the gene score resampling method. We used the standard gene sets available through ErmineJ, which are based in GeneOntology, and statistical scores were calculated for these sets. For IPA, the probe sets, -fold change, and *P* values from the RMA analysis of the P45 and P90 amygdalar gene arrays were entered. To allow for detection of relatively subtle, but still reliable, differences in gene expression, genes showing a greater than 1.2-fold change at a significance level of a $P < 0.05$ were retained for analysis. From this data set, relevant "biological functions" were identified. The IPA "biological functions" gene sets were determined on the basis of proprietary literature search algorithms by Ingenuity.

RESULTS

BA-projecting neurons in the mPFC decrease in number during late adolescence or early adulthood

Matching the location and size of the tracer deposit across different-aged brains—We used the matching criteria described in Materials and Methods to identify three P25 and four P90 brains from experiment 1 (from 32 subjects) with nearly identical FG injection locations and sizes. The extent and location of the injection sites of these cases are represented schematically in Figure 2. Injection site volumes did not differ between P25 and P90 brains [mm^3, mean ± SEM: P25, 0.94 ± 0.32; P90, 1.11 ± 0.15; $t(5) = 0.33$, $P > 0.7$]. Similarly, in experiment 2, five brains with injections of FG at P25, six brains at P45, and five brains at P90 were selected based on similarities in the location and spread of FG. The location and size of these injection sites within the BA are depicted schematically in Figure

3. Photomicrographs of the injection sites for representative animals at each age are provided in Supporting Information Figure 1. There were no significant differences in the volume of the injection within the BA [mm^3, mean ± SEM: P25, 1.26 ± 0.23; P45, 1.40 ± 0.21; P90, 1.26 ± 0.23; $F(2,13) = 0.15$, $P > 0.8$]. In both experiments, labeling along the injection tract was minimal, with a few labeled cells observed primarily at the site of entry and occasional cells in the injection track.

Decreases in BA-projecting neurons in the mPFC between late adolescence and adulthood—There were small, nonsignificant decreases in the volume of the mPFC between P25 and P90 for both experiment 1 [mm^3, mean ± SEM: P25, 6.6 ± 0.4; P90, 6.1 ± 0.5; $t(5) = 0.85$, $P > 0.4$] and experiment 2 [mm^3, mean ± SEM: P25, 6.8 ± 0.4; P45, 6.9 ± 0.3; P90, 6.1 ± 0.4; $F(2,13) = 1.6$, $P > 0.2$]. The small decrease is consistent with previous reports (Van Eden and Uylings, 1985).

Experiment 1 showed a significant, approximately 50% reduction in the number of FG-labeled cells in the mPFC between P25 (n = 3) and P90 [n = 4; $F(2,1,4) = 10.7$, $P < 0.05$; Fig. 4A]. Similarly, in experiment 2, the number of retrogradely labeled neurons in the mPFC was significantly different among the age groups [$F(2,1,12) = 14.9$, $P < 0.001$; Fig. 4B]. Post hoc contrasts revealed no significant change between P25 (n = 5) and P45 (n = 6; $P = 0.46$) but a significant decrease between P45 and P90 (n = 5; $P < 0.001$). We note that, although overall labeling appeared to be more robust with the 14-day survival period, the level of labeling after the 4-day survival was significant and reliable (see Supporting Information Fig. 3). Moreover, the relative decrease in BA-projecting neurons in the PFC between P25 and P90 was remarkably similar for both survival periods. Thus, these experiments have revealed an age-related decrease in the number of neurons projecting to the BA that is not confounded by an artifact of age-related differences in axonal transport efficiency.

Subregional analysis of age-related changes in retrograde labeling—Generally, the topographic distribution of retrogradely labeled mPFC cells appeared to be similar across ages and consistent with previous descriptions (Cassell and Wright, 1986; Gabbott et al., 2005). Within the mPFC, the quantity of FG-labeled neurons increased in the rostral-to-caudal and dorsal-to-ventral directions. Labeled cells were seen in both superficial layer 2 and deep layer 5 in all subdivisions of the mPFC (Fig. 5A–C). A composite of these patterns for all of the animals analyzed is diagramed onto representative sections in Figure 5A–C in colors corresponding to the injection site for each case represented in Figure 3. Developmental patterns within subregions were explored with an alternate analysis of the data using a mixed ANOVA with the age as the between-subjects factor, the mPFC subregion as the within-subjects variable, and the injection volume as the covariate. This analysis revealed the expected significant main effect of age [$F(2,1,12) = 14.9$, $P = 0.001$] but also a significant age × subregion interaction [$F(4,2,24) = 3.5$, $P < 0.05$; Fig. 5D]. The basis for this interaction was explored by performing two pairwise contrasts per subregion: P25 vs. P45 and P45 vs. P90. Labeling in the IL showed a nonsignificant decrease between P25 and P45 ($P = 0.19$), followed by a significant decrease between P45 and P90 ($P < 0.05$). The ACg showed a similar but nonsignificant pattern of age-related changes. By contrast, labeling in the PL showed a nonsignificant increase in BA-projecting neurons between P25 and P45 ($P = 0.24$), followed by a highly significant decline between P45 and P90 ($P < 0.01$).

The decline in BA-projecting mPFC neurons between late adolescence and adulthood is accompanied by decreased density of mPFC-derived axonal terminals in the BA

Identification of case series with equivalent BDA deposits in the mPFC in late juvenile, late adolescent, and adult cases—The oblong nature and large size of the mPFC contributed to a considerable level of variability in the injection sizes and locations across all three age groups. Among the 81 animals injected, we identified two sets of brains with similar injection sizes and locations. In the first set, injection sites in P25 (n = 3), P45 (n = 4), and P90 (n = 3) brains were nearly identical. In the second set, the injection sites of P45 (n = 2) and P90 (n = 2) brains were matched but were slightly larger than the sites in P25 brains (n = 2). All injection sites were located primarily in the ventral prelimbic and dorsal infralimbic cortices. The extent and location of the injection sites in the mPFC for representative cases are shown in in Figure 6. Representative contours used in the evaluation of the tracer deposit volume are superimposed upon the corresponding photomicrographs in Supporting Information Figure 2. Average volumes of BDA uptake across both sets did not differ among age groups [mm^3, mean ± SEM: P25, 1.1 ± 0.2; P45, 1.2 ± 0.2; P90, 1.5 ± 0.2; $F(2,13) = 1.4$, $P > 0.25$].

Changes in the mPFC innervation of the BA between adolescence and adulthood—The average volume of the BA did not differ across age groups (in mm^3, mean ± SEM: P25, 8.2 ± 0.41; P45, 7.7 ± 0.38; P90, 8.2 ± 0.41; $P > 0.6$). However, the density of mPFC-derived axon terminals in the BA was decreased in adulthood, relative to early (P25) or late (P45) adolescence. A representative example of the approximate distribution of the fibers as assessed by systematic random sampling is shown for each of the three age groups in Figure 7. Anterograde labeling from the mPFC sites shown in Figure 6 was most dense in the dorsomedial portion of the basolateral nucleus of the amygdala (Figs. 7, 8A,C–H). As a result of slight variations in injection sites in the two sets used for the analysis, the ANOVA analyzed fiber density (fiber length/mPFC volume) as a function of age group and injection site set, using injection site volume as a covariate. This analysis was used to test the hypothesis generated by the retrograde tracing experiment, that mPFC axonal fiber density in the BA would be significantly greater at P25 and P45 than at P90. Quantification revealed no main effect of injection site location ($P > 0.18$) but showed a significant age-related reduction in the estimated total length of BDA-labeled fibers within the BA [$F(2,1,9) = 3.7$, $P < 0.05$]. Pairwise contrasts showed no changes in mPFC fiber density between P25 and P45 (one-tailed $P > 0.4$) but a significant decrease in fiber density at P90 relative to either P45 (one-tailed $P < 0.02$) or P25 (one-tailed $P < 0.025$; Fig. 8B).

We note that the density of anterogradely labeled fibers from the mPFC in the BA appeared to be lower at all ages in this study than that shown in previous studies of the adult (McDonald et al., 1996; Vertes, 2004), perhaps as a result of differences in anterograde tracer [BDA vs. *Phaseolus vulgaris* leucoagglutinin (PHAL)] or in the deposit (size) or uptake of tracer. The decrease in labeling, relative to images shown in previous studies using PHAL (Sesack et al., 1989), was also apparent in other PFC efferent systems, such as fibers in ventral tegmental area, regions that showed no apparent age-related differences in the current study (data not shown). Thus, it is unlikely that there were general age-related differences in tracer uptake, transport, or labeling contributing to the above results. We also note that we rarely observed neurons in the BA retrogradely labeled with BDA. When observed, such neurons were located lateral and/or ventral to the region of highest fiber density in the BA. However, examination of this case series, as well as the remaining brains with mPFC-derived anterograde labeling in the BA (45 brains; data not shown) revealed no relationship between the number or location of retrogradely labeled soma and the density of labeled fibers in the dorsomedial BA. Thus, although a small number of fibers may represent

axon collaterals of retrogradely labeled neurons (Pitkanen, 2000), we expect that this is an insignificant proportion of the total labeling.

Gene expression profiles provide molecular evidence for changes in neurite remodeling in the BA between late adolescence and adulthood

Among the 31,000 probe sets covering 28,000 genes on the Affymetrix Rat 230 2.0 gene array, the majority (82%) differed by less than 20%. Among the probes with an absolute -fold change greater than 1.2, 3,912 probes were higher in the P45 amygdala compared with the P90 amygdala, whereas 1,736 probes were higher in the P90 amygdala. Only 45 probes (0.14%) differed by greater than twofold.

Age-related changes in gene expression were first anayzed by using ErmineJ (Lee et al., 2005), an approach that detects statistically significant changes in GeneOntology groups. The vast majority of functional groups specific to mature neuronal function were not significantly altered (corrected Ps > 0.05). These included the following: neurotransmitter transport and secretion pathways; glutamatergic, dopaminergic, serotonergic and GABA receptor-related pathways; voltage-gated calcium and potassium channels; and synaptic vesicle endocytosis/exocytosis or transport pathways. Moreover, pathways activated in earlier stages of development, such as neuron migration, neuron fate commitment, neurogenesis regulation, midbrain development, and regulation of dendrite development, were also not significantly changed. Instead, the 18 most significant GeneOntology groups, each with a P value of 10^{-13}, centered around three clusters of GeneOntology groups involving 1) modulation of the cytoskeleton, 2) steroid syntheses and processes, and 3) Ras/GTP related proteins. The cytoskeletal cluster comprised six GeneOntology groups: actin cytoskeleton organization and biogenesis, microtubule-based process, actin binding, actin filament-based process, axon, and neurite development. The lipid metabolism and steroid-related processes cluster included the GeneOntology groups cholesterol biosynthetic process, sterol biosynthetic process, steroid biosynthetic process, and steroid metabolic process. The Ras/GTP-related protein cluster included the three GeneOntology groups GTPase activity, small GTPase-mediated signal transduction, and Ras protein signal transduction. Specifically, significant expression changes between P45 and P90 were seen in 25 genes in the cytoskeletal cluster, 12 genes in the Ras/GTP-related cluster, and 13 genes in the lipid metabolism and steroid-related processes cluster. Table 2 lists the genes in each category with a statistical significance of $P < 0.02$. Proteins within each of these three clusters have been implicated in neurite outgrowth and retraction.

The RMA output was also independently analyzed with IPA, focusing on identifying potential relevant changes in biological functions. With this approach, the eight most significant biological functions were cellular assembly and organization, cellular compromise, development (embryonic development, tissue development, nervous system development, and organ development), tissue morphology, and lipid metabolism. Within the cellular assembly and organization, 20 genes identified as having statistically different expression levels were identified. Although many similar genes were noted in both ErmineJ and IPA for corresponding biological functions, unique genes in these pathways were identified in each analysis. Supporting Information Table 1 lists genes in cytoskeleton-, steroid-, or Ras/GTPase-relevant categories that showed a statistically significant change of greater than 1.2-fold as identified by ErmineJ or IPA and distinguishes additional genes found with only one of the two analysis systems.

DISCUSSION

The anatomical and gene expression profiling experiments described herein provide evidence that, during the transition from adolescence to adulthood in the rat, there is

significant structural remodeling of the mPFC inputs to the BA that is accompanied by molecular changes related to neurite plasticity within BA cells.

Axonal remodeling in mPFC-amygdalar circuits during late adolescence

The present tract-tracing data highlight the value of a circuit-based approach to studying the adolescent brain and represent information that can be gained only through examination of connectivity between regions of interest. As such, the present data show that mPFC inputs to the BA remain relatively stable between early and late adolescence and then decrease dramatically during the transition to adulthood. These findings can be integrated with those of Bouwmeester et al. (2002), who examined the PFC innervation of the basolateral amygdala between P7 through P21 using retrograde tracing methods. In their report, the distribution of BA-projecting cells in the mPFC expanded dorsally and into a bilaminar pattern during this period. The patterns of retrograde labeling in the mPFC that were observed at P25 in the current study are consistent with the patterns that Bouwmeester et al. observed at P21, and the distribution of labeling in our P90 cases is similar to that in previous reports with adult rats (Cassell and Wright, 1986). Taking these studies and our current findings together, we estimate that the mPFC projection to the BA may increase through early adolescence, plateau during adolescence, and then undergo pruning between late adolescence and adulthood.

The current study also provides novel evidence that approximately half of the neurons projecting to the BA from the mPFC in the juvenile brain fully retract their axons from the BA between late adolescence and adulthood. This is supported by the remarkable similarity between the degree of loss of BA-projecting neurons in the mPFC and the loss of mPFC-derived fibers in the BA over the same developmental period. Moreover, our subregional analysis provides preliminary evidence that adolescent-associated reductions in BA projections may occur to a relatively greater extent, or with a different time course, in the PL, relative to the IL/DP or ACg. Although this post hoc analysis should be interpreted with caution, it provides a rationale for testing the hypothesis that there is subcircuit specificity in the developmental curves for PFC-amygdala circuits as they undergo remodeling during adolescence.

There is a small (5%) overall loss of neurons in the mPFC during adolescence (Markham et al., 2007), so neuronal loss might have contributed to our findings. Along these lines, it would be interesting to examine the possibility that the small loss of neurons in the PFC during adolescence is not uniform but represents disproportionate culling of specific circuits. Although it would be difficult to test this hypothesis directly, it leads to a related prediction that, during adolescence, a portion of the neurons retrogradely labeled from the BA undergoes (and exhibit markers of) cell death. An alternative interpretation is that a large group of mPFC neurons projecting to the BA do not die, but retract their axons from the BA after P45. Exuberant innervation of subcortical structures followed by axonal retraction from a subset of these targets is a common motif in the development of cortical efferents, as exhibited by some cortical efferents in early postnatal development (Clarke and Innocenti, 1986; Luo and O'Leary, 2005; Schreyer and Jones, 1988). We speculate that mPFC efferents to the limbic forebrain may be programmed to follow this motif during adolescence. Collateralization of PFC axons to multiple subcortical targets is infrequent in the adult brain (Pinto and Sesack, 2000). However, given the current data, there may be a greater frequency of such collateralization until adolescence, after which some mPFC neurons retract their axons from the BA while continuing to innervate a smaller set of targets in adulthood. In other systems, both ingrowth and elimination of cortical axons during development are postulated to be modulated by experience and circuit activity (Friel and Martin, 2005; Luo and O'Leary, 2005). In the case of the mPFC-BA circuit, an additional possibility is that the retraction of mPFC-projecting fibers is associated with the neuronal

cell loss in the BA seen during this period (Rubinow and Juraska, 2009). This would again suggest circuit specificity in the nature of the cell loss, specifically, that the BA neurons lost are those from which PFC inputs have with-drawn. The direction of the causal association (i.e., whether the BA neuronal loss results in mPFC fiber retraction or vice versa) requires further study. Finally, mPFC axonal retraction may be influenced by developmental changes in subcortical inputs to the mPFC, particularly those from the BA (Cunningham et al., 2002), such that changes in signals from amygdalar or other afferents to the mPFC may contribute to the selection of mPFC neurons that remain connected with the BA.

Identification of candidate molecular pathways mediating neurite remodeling during adolescence

Two complementary methods for pathway analysis of gene expression array data independently identified three molecular pathways that were highly differentially expressed in late adolescence relative to adulthood: Ras/GTPase, cytoskeleton regulation, and lipid metabolism and steroid-related processes. Each of these pathways is important in the regulation of neurite modeling. Gene expression in the majority of neuron-specific pathways did *not* differ in the adolescent and adult BA; rather, age-related differences were selective for these three functional groups. To date, studies of molecular mechanisms of axonal pruning have focused on individual cornerstone molecules (e.g., semaphorins/ephrins; Bagri et al., 2003). Our findings demonstrate that the complementary approach of using gene expression profiling may identify molecular pathways that could potentially mediate neurite remodeling in adolescence. Moreover, the use of multiple bioinformatic modeling systems can provide consensus on the most reliably changed and functionally significant molecular pathways.

Although discussion of the roles of individual genes in neurite remodeling is beyond the scope of this report, it is useful to consider the implications of the functional families that show significant age-related changes in regulation between adolescence and adulthood. Figure 9 provides an overview of potential roles for the three functional groups that were the most differentially expressed in the late adolescent and adult BA. The cytoskeletal functional group includes proteins that are structural components of neurites, and regulators of polymerization and depolymerization of these components. The lipid metabolism and steroid-related processes includes enzymes responsible for cholesterol biosynthesis and impact the integration of cholesterol into the membrane of the neurite (Pfrieger, 2003), specifically, at the synaptic cleft. This pathway may be involved in regulating the response of the postsynaptic membrane to the retraction of an axonal apposition or synaptic input. The Ras/GTPase superfamily proteins, including their regulators and effectors, regulate presynaptic and postsynaptic (e.g., spine) neurite outgrowth and specialization as well as synaptic plasticity (Arendt et al., 2004;Kushner et al., 2005;Seeger et al., 2005;Yang and Mattingly, 2006). Further analysis will reveal how these gene expression changes relate to structural remodeling of neurites and/or synaptic plasticity in the amygdala during adolescence. Although the changes in gene expression described above are not conclusive evidence for neurite remodeling in the BA during late adolescence, this interpretation is consistent with our observation of pruning of BA afferents and with a recent report of decreased neuron and glia number in the basolateral amygdala between P35 and P90 (Rubinow and Juraska, 2009). In conjunction, these two studies suggest that the afferent connectivity to the BA is highly dynamic during adolescence.

Implications for psychological development and the vulnerability for psychopathology in adolescence and early adulthood

The current findings are consistent with other studies showing that structural and functional development of PFC and limbic-related circuits can be more protracted than that of their

sensory counterparts (Casey et al., 2008; Lavenex et al., 2007; Monk et al., 2003). As part of this development, genes regulating neurite plasticity may be uniquely regulated during adolescence to maintain the capacity for axonal and/or dendritic remodeling (see Fig. 9; Luo and O'Leary, 2005). This may be functionally related to the nature of behavioral transitions associated with adolescence, which involve increases in independent foraging and social approach behaviors. These behaviors are necessary for survival and procreation but also increase the exposure of the organism to potential threats. Thus, adolescence may necessitate a change in affective regulation that increases the organism's tolerance for risk (Casey et al., 2008; Spear, 2000). Accordingly, the circuits mediating these adaptive processes must maintain a degree of plasticity during adolescence. Along these lines, the mPFC modulates habituation to repeated stress and appraisal of potential threats (Quirk et al., 2006). Such habituation is less reliable in juvenile rats relative to adults (Romeo et al., 2006), and it may be speculated that adolescent changes in mPFC-amygdalar connectivity assist in the habituation of exposure to repeated stressors. The mPFC-amygdalar circuit also regulates extinction of conditioned fear and consolidation of extinction memories (Quirk et al., 2006; Sotres-Bayon et al., 2004). Moreover, the sensitivity of the mPFC to stress (unconditioned fear) also emerges between the juvenile and the adolescent periods (Andersen et al., 2008; Leussis et al., 2008). In this context, it is notable that synaptic plasticity underlying amygdala-mediated fear conditioning and memory is regulated by Ras signaling pathways (Brambilla et al., 1997; Merino and Maren, 2006; Ou and Gean, 2006). Thus, pruning of mPFC inputs may be one aspect of plasticity in BA circuitry, regulated by Ras signaling pathways, that leads to changes in the regulation of learned fear-related behavior during adolescence.

In summary, we believe this study provides support for the postulate that remodeling of the mPFC inputs to the BA, and perhaps within other corticolimbic circuits, may be an important phase in brain development that normally occurs during adolescence. Moreover, this process may be critical for the organism's ability to respond to the unique challenges associated with the transition to adulthood. Disruption of this process could lead to a loss of normal afferent regulation of amygdalar activity (Blakemore and Choudhury, 2006) and inappropriate amygdalar drive of behavioral effector circuits (Johnstone et al., 2007). Such abnormalities have been postulated to contribute to the psychopathology of a number of psychiatric disorders. Thus, determining the molecular mechanisms underlying structural plasticity in adolescent limbic circuits will lead to a deeper understanding of the adaptive, as well as pathological, behavioral changes that occur during adolescence.

Supplementary Material

Refer to Web version on PubMed Central for supplementary material.

Acknowledgments

The authors thank Jennifer Perusini, for her assistance with microscopy and stereology and Paul Pavlidis, PhD, for public access to and training on the use of ErmineJ (http://bioinformatics.ubc.ca/ermineJ).

Grant sponsor: Lieber Center for Schizophrenia Research at Columbia University (to H.M.); Gatsby Initiative in Brain Circuitry (to H.M.); Public Health Service; Grant number: MH 66171 (to H.M.); Grant number: T32 Fellowship MH 18879 (to V.L.C.); Grant sponsor: Paul Janssen Fellowship in Translational Research (to V.L.C.).

LITERATURE CITED

Aleman A, Kahn RS. Strange feelings: do amygdala abnormalities dysregulate the emotional brain in schizophrenia? Prog Neurobiol. 2005; 77:283–298. [PubMed: 16352388]

Amsel A, Chen JS. Ontogeny of persistence: immediate and long-term persistence in rats varying in training age between 17 and 65 days. J Comp Physiol Psychol. 1976; 90:808–820. [PubMed: 965529]

Andersen SL, Thompson AP, Krenzel E, Teicher MH. Pubertal changes in gonadal hormones do not underlie adolescent dopamine receptor overproduction. Psychoneuroendocrinology. 2002; 27:683–691. [PubMed: 12084661]

Andersen SL, Tomada A, Vincow ES, Valente E, Polcari A, Teicher MH. Preliminary evidence for sensitive periods in the effect of childhood sexual abuse on regional brain development. J Neuropsychiatry Clin Neurosci. 2008; 20:292–301. [PubMed: 18806232]

Arendt T, Gartner U, Seeger G, Barmashenko G, Palm K, Mittmann T, Yan L, Hummeke M, Behrbohm J, Bruckner MK, Holzer M, Wahle P, Heumann R. Neuronal activation of Ras regulates synaptic connectivity. Eur J Neurosci. 2004; 19:2953–2966. [PubMed: 15182302]

Bagri A, Cheng H-J, Yaron A, Pleasure SJ, Tessier-Lavigne M. Stereotyped pruning of long hippocampal axon branches triggered by retraction inducers of the semaphorin family. Cell. 2003; 113:285–299. [PubMed: 12732138]

Blakemore SJ, Choudhury S. Development of the adolescent brain: implications for executive function and social cognition. J Child Psychol Psychiatry. 2006; 47:296–312. [PubMed: 16492261]

Blumberg HP, Kaufman J, Martin A, Charney DS, Krystal JH, Peterson BS. Significance of adolescent neurodevelopment for the neural circuitry of bipolar disorder. Ann N Y Acad Sci. 2004; 1021:376–383. [PubMed: 15251913]

Bouwmeester H, Smits K, Van Ree JM. Neonatal development of projections to the basolateral amygdala from prefrontal and thalamic structures in rat. J Comp Neurol. 2002; 450:241–255. [PubMed: 12209853]

Brambilla R, Gnesutta N, Minichiello L, White G, Roylance AJ, Herron CE, Ramsey M, Wolfer DP, Cestari V, Rossi-Arnaud C, Grant SG, Chapman PF, Lipp HP, Sturani E, Klein R. A role for the Ras signalling pathway in synaptic transmission and long-term memory. Nature. 1997; 390:281–286. [PubMed: 9384379]

Casey, BJ.; Jones, RM.; Hare, TA. The year in cognitive neuroscience 2008. New York Academy of Sciences; New York: 2008. The adolescent brain; p. 111-126.

Cassell MD, Wright DJ. Topography of projections from the medial prefrontal cortex to the amygdala in the rat. Brain Res Bull. 1986; 17:321–333. [PubMed: 2429740]

Clarke S, Innocenti GM. Organization of immature intrahemispheric connections. J Comp Neurol. 1986; 251:1–22. [PubMed: 3760253]

Cunningham MG, Bhattacharyya S, Benes FM. Amygdalo-cortical sprouting continues into early adulthood: implications for the development of normal and abnormal function during adolescence. J Comp Neurol. 2002; 453:116–130. [PubMed: 12373778]

Cunningham MG, Bhattacharyya S, Benes FM. Increasing interaction of amygdalar afferents with GABAergic interneurons between birth and adulthood. Cereb Cortex. 2007; 18:1529–1935. [PubMed: 17971342]

Drevets WC. Neuroimaging abnormalities in the amygdala in mood disorders. Ann NY Acad Sci. 2003; 985:420–444. [PubMed: 12724175]

Elston GN, Oga T, Fujita I. Spinogenesis and pruning scales across functional hierarchies. J Neurosci. 2009; 29:3271–3275. [PubMed: 19279264]

Friel KM, Martin JH. Role of sensory-motor cortex activity in postnatal development of corticospinal axon terminals in the cat. J Comp Neurol. 2005; 485:43–56. [PubMed: 15776437]

Gabbott PL, Warner TA, Jays PR, Salway P, Busby SJ. Prefrontal cortex in the rat: projections to subcortical autonomic, motor, and limbic centers. J Comp Neurol. 2005; 492:145–177. [PubMed: 16196030]

Guyer AE, Monk CS, McClure-Tone EB, Nelson EE, Roberson-Nay R, Adler AD, Fromm SJ, Leibenluft E, Pine DS, Ernst M. A developmental examination of amygdala response to facial expressions. J Cogn Neurosci. 2008; 20:1565–1582. [PubMed: 18345988]

Hare TA, Tottenham N, Galvan A, Voss HU, Glover GH, Casey BJ. Biological substrates of emotional reactivity and regulation in adolescence during an emotional go-nogo task. Biol Psychiatry. 2008; 63:927–934. [PubMed: 18452757]

Johnstone T, van Reekum CM, Urry HL, Kalin NH, Davidson RJ. Failure to regulate: counterproductive recruitment of top-down prefrontal-subcortical circuitry in major depression. J Neurosci. 2007; 27:8877–8884. [PubMed: 17699669]

Kessler RC, Berglund P, Demler O, Jin R, Merikangas KR, Walters EE. Lifetime prevalence and age-of-onset distributions of DSM-IV disorders in the National Comorbidity Survey Replication. Arch Gen Psychiatry. 2005; 62:593–602. [PubMed: 15939837]

Koshibu K, Levitt P, Ahrens ET. Sex-specific, postpuberty changes in mouse brain structures revealed by threedimensional magnetic resonance microscopy. Neuroimage. 2004; 22:1636–1645. [PubMed: 15275920]

Kushner SA, Elgersma Y, Murphy GG, Jaarsma D, van Woerden GM, Hojjati MR, Cui Y, LeBoutillier JC, Marrone DF, Choi ES, De Zeeuw CI, Petit TL, Pozzo-Miller L, Silva AJ. Modulation of presynaptic plasticity and learning by the H-ras/extracellular signal-regulated kinase/synapsin I signaling pathway. J Neurosci. 2005; 25:9721–9734. [PubMed: 16237176]

Lavenex P, Banta Lavenex P, Amaral DG. Postnatal development of the primate hippocampal formation. Dev Neurosci. 2007; 29:179–192. [PubMed: 17148960]

Lee HK, Braynen W, Keshav K, Pavlidis P. ErmineJ: tool for functional analysis of gene expression data sets. BMC Bioinformatics. 2005; 6:269. [PubMed: 16280084]

Leussis MP, Lawson K, Stone K, Andersen SL. The enduring effects of an adolescent social stressor on synaptic density, part II: poststress reversal of synaptic loss in the cortex by adinazolam and MK-801. Synapse. 2008; 62:185–192. [PubMed: 18081181]

Lewis DA, Cruz D, Eggan S, Erickson S. Postnatal development of prefrontal inhibitory circuits and the pathophysiology of cognitive dysfunction in schizophrenia. Ann NY Acad Sci. 2004; 1021:64–76. [PubMed: 15251876]

Luo L, O'Leary DD. Axon retraction and degeneration in development and disease. Annu Rev Neurosci. 2005; 28:127–156. [PubMed: 16022592]

Markham JA, Morris JR, Juraska JM. Neuron number decreases in the rat ventral, but not dorsal, medial prefrontal cortex between adolescence and adulthood. Neuroscience. 2007; 144:961–968. [PubMed: 17137726]

McDonald AJ, Mascagni F, Guo L. Projections of the medial and lateral prefrontal cortices to the amygdala: a *Phaseolus vulgaris* leucoagglutinin study in the rat. Neuroscience. 1996; 71:55–75. [PubMed: 8834392]

McDonald AJ, Shammah-Lagnado SJ, Shi C, Davis M. Cortical afferents to the extended amygdala. Ann NY Acad Sci. 1999; 877:309–338. [PubMed: 10415657]

Merino SM, Maren S. Hitting Ras where it counts: Ras antagonism in the basolateral amygdala inhibits long-term fear memory. Eur J Neurosci. 2006; 23:196–204. [PubMed: 16420429]

Monk CS, McClure EB, Nelson EE, Zarahn E, Bilder RM, Leibenluft E, Charney DS, Ernst M, Pine DS. Adolescent immaturity in attention-related brain engagement to emotional facial expressions. Neuroimage. 2003; 20:420–428. [PubMed: 14527602]

Mouton, PR. Principles and practices of unbiased stereology: an introduction for bioscientists. Johns Hopkins University Press; Baltimore: 2002.

Ou LC, Gean PW. Regulation of amygdala-dependent learning by brain-derived neurotrophic factor is mediated by extracellular signal-regulated kinase and phosphatidylinositol-3-kinase. Neuropsychopharmacology. 2006; 31:287–296. [PubMed: 16034442]

Paus T, Keshavan M, Giedd JN. Why do many psychiatric disorders emerge during adolescence? Nat Rev Neurosci. 2008; 9:947–957. [PubMed: 19002191]

Paxinos, G. The rat nervous system. Academic Press; San Diego: 1995.

Paxinos, G.; Watson, C. The rat brain in stereotaxic coordinates. 4th ed. Academic Press; New York: 1998.

Pfrieger FW. Role of cholesterol in synapse formation and function. Biochim Biophys Acta. 2003; 1610:271–280. [PubMed: 12648780]

Phillips ML, Drevets WC, Rauch SL, Lane R. Neurobiology of emotion perception II: Implications for major psychiatric disorders. Biol Psychiatry. 2003; 54:515–528. [PubMed: 12946880]

Pinto A, Sesack SR. Limited collateralization of neurons in the rat prefrontal cortex that project to the nucleus accumbens. Neuroscience. 2000; 97:635–642. [PubMed: 10842008]

Pitkanen, A. Connectivity of the rat amygdaloid complex. In: Aggleton, JP., editor. The amygdala: a functional analysis. Oxford University Press; New York: 2000. p. 31-116.

Quirk GJ, Garcia R, Gonzalez-Lima F. Prefrontal mechanisms in extinction of conditioned fear. Biol Psychiatry. 2006; 60:337–343. [PubMed: 16712801]

Rakic, P.; Bourgeois, JP.; Goldman-Rakic, PS. Synaptic development of the cerebral cortex: implications for learning, memory, and mental illness. In: van Pelt, J.; Corner, MA.; Uylings, HBM.; da Silva, FH Lopes, editors. Progress in brain research. The self-organizing brain: from growth cones to functional networks. Elsevier; Amsterdam: 1994. p. 227-243.

Romeo RD, Bellani R, Karatsoreos IN, Chhua N, Vernov M, Conrad CD, McEwen BS. Stress history and pubertal development interact to shape hypothalamic-pituitary-adrenal axis plasticity. Endocrinology. 2006; 147:1664–1674. [PubMed: 16410296]

Rubinow MJ, Juraska JM. Neuron and glia numbers in the basolateral nucleus of the amygdala from preweaning through old age in male and female rats: a stereological study. J Comp Neurol. 2009; 512:717–725. [PubMed: 19065620]

Schreyer DJ, Jones EG. Axon elimination in the developing corticospinal tract of the rat [erratum appears in Brain Res 467:320, 1988]. Brain Res. 1988; 466:103–119. [PubMed: 3342323]

Seeger G, Gartner U, Arendt T. Transgenic activation of Ras in neurons increases synapse formation in mouse neocortex. J Neural Transm. 2005; 112:751–761. [PubMed: 15480849]

Sesack SR, Deutch AY, Roth RH, Bunney BS. Topographical organization of the efferent projections of the medial prefrontal cortex in the rat: an anterograde tracttracing study with *Phaseolus vulgaris* leucoagglutinin. J Comp Neurol. 1989; 290:213–242. [PubMed: 2592611]

Sotres-Bayon F, Bush DE, LeDoux JE. Emotional perseveration: an update on prefrontal-amygdala interactions in fear extinction. Learn Mem. 2004; 11:525–535. [PubMed: 15466303]

Spear LP. The adolescent brain and age-related behavioral manifestations. Neurosci Biobehav Rev. 2000; 24:417–463. [PubMed: 10817843]

Tessier-Lavigne M, Goodman CS. The molecular biology of axon guidance. Science. 1996; 274:1123–1133. [PubMed: 8895455]

Van Eden CG, Uylings HB. Postnatal volumetric development of the prefrontal cortex in the rat. J Comp Neurol. 1985; 241:268–274. [PubMed: 4086657]

Vertes RP. Differential projections of the infralimbic and prelimbic cortex in the rat. Synapse. 2004; 51:32–58. [PubMed: 14579424]

Woo TU, Pucak ML, Kye CH, Matus CV, Lewis DA. Peripubertal refinement of the intrinsic and associational circuitry in monkey prefrontal cortex. Neuroscience. 1997; 80:1149–1158. [PubMed: 9284067]

Yang H, Mattingly RR. The Ras-GRF1 exchange factor coordinates activation of H-Ras and Rac1 to control neuronal morphology. Mol Biol Cell. 2006; 17:2177–2189. [PubMed: 16481401]

Zehr JL, Todd BJ, Schulz KM, McCarthy MM, Sisk CL. Dendritic pruning of the medial amygdala during pubertal development of the male Syrian hamster. J Neurobiol. 2006; 66:578–590. [PubMed: 16555234]

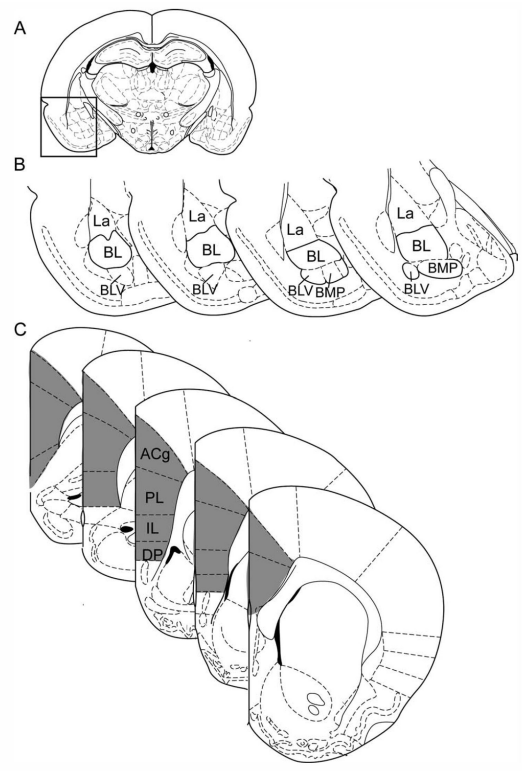

Figure 1.

Regions of interest: the basal amygdala and the medial prefrontal cortex. Schematic diagrams of the regions of interest (ROIs) for the basal amygdala (BA; **A,B**) and the medial prefrontal cortex (mPFC; **C**) at representative coronal levels. The schematic of the full brain at a coronal level containing the center of the BA ROI is shown in A; the boxed region is magnified in B. The BA ROI, as shown in B, encompassed the anterior and posterior basolateral amygdalar nucleus (BL) and the caudal portions of the ventral basolateral (BLV) and posterior basomedial (BMP) nuclei. The lateral nucleus (La) and rostral BLV were not included. The mPFC ROI, shaded in gray in C, included the anterior cingulate (ACg), prelimbic (PL), infralimbic (IL), and dorsal peduncular (DP) regions. All schematics in this and subsequent figures, with the exception of Supporting Information Figure 2, were modified from Paxinos and Watson (1998).

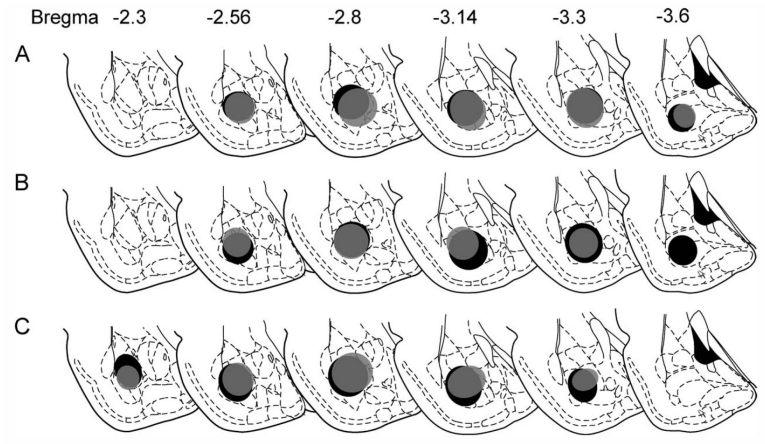

Figure 2.

Comparison across age groups of retrograde tracer deposits within the BA for experiment 1. Fluorogold (FG) was injected into the BA at P25 (gray) or P90 (black), and brains were collected 14 days later. **A–C** show injection sites for sets of P25 and P90 brains determined to have matched injection sites. Quantification of retrograde labeling in the mPFC of these brains is shown in Figure 4A.

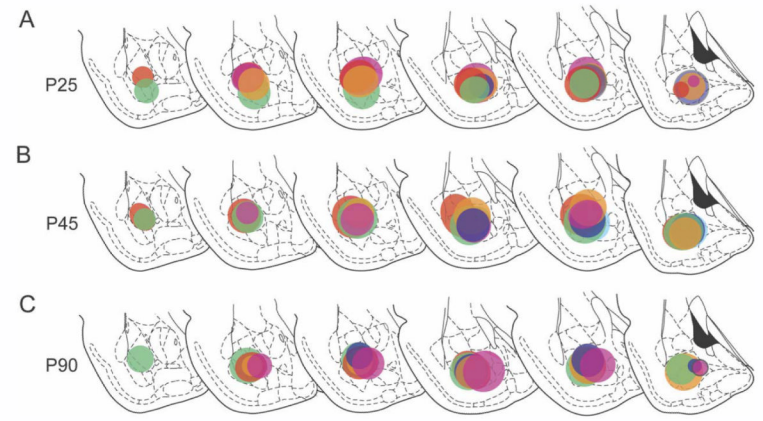

Figure 3.

Comparison across age groups of retrograde tracer deposits within the BA for experiment 2. The location and extent of the FG injection and estimated uptake within the BA following a 4-day survival period for animals injected at P25 (**A**), P45 (**B**), and P90 (**C**). Quantification of retrograde labeling in the mPFC of these brains is shown in Figure 4B.

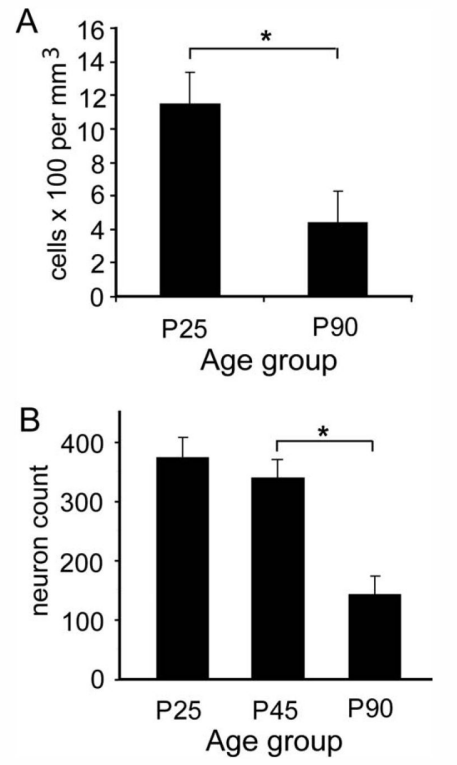

Figure 4.

Reduction in the number of retrogradely labeled cells in the mPFC occurring between late adolescence and adulthood. **A**: Experiment 1. The density of FG-labeled cells in the mPFC (mean ± SEM) 14 days following iontophoresis of FG into the BA at P25 (n = 3) or P90 (n = 4). Injection sites for these cases are shown in Figure 2. **B**: Experiment 2. The number of FG-labeled cells (mean ± SEM; standardized by sampling area) in mPFC 4 days following iontophoresis of FG into the BA at P25 (n = 5), P45 (n = 6), or P90 (n = 5). Injection sites for these cases are shown in Figure 3. *$P < 0.05$, pairwise contrast.

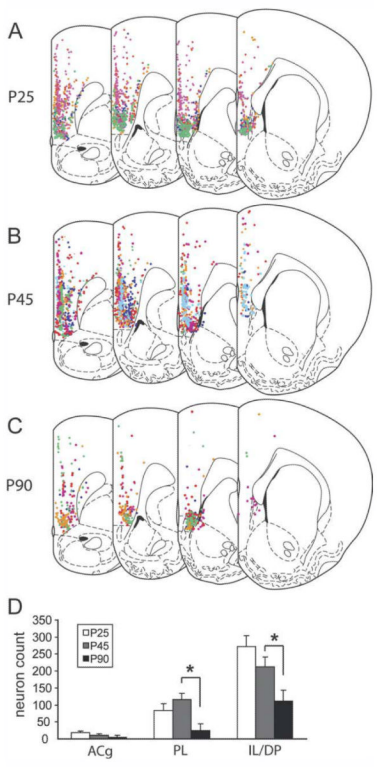

Figure 5.

Distribution and subregional quantification of the BA-projecting neurons in the mPFC at P25, P45, and P90. **A–C**: The distribution, mapped onto representative coronal levels, of all neurons retrogradely labeled from the injection sites shown in Figure 3. For each case, retrogradely labeled neurons in the mPFC are shown in the color corresponding to the injection site in Figure 3. **D**: Reanalysis of the data from experiment 2 with a design that included mPFC subregion as a within-subject factor revealed a significant age × subregion analysis. Although the only significant changes are decreases in BA-projecting neurons in IL/DP and PL between P45 and P90, the overall pattern of age-related changes appeared to be different in the PL from that in either AC or IL/DP (see text). $*P < 0.05$, pairwise contrast.

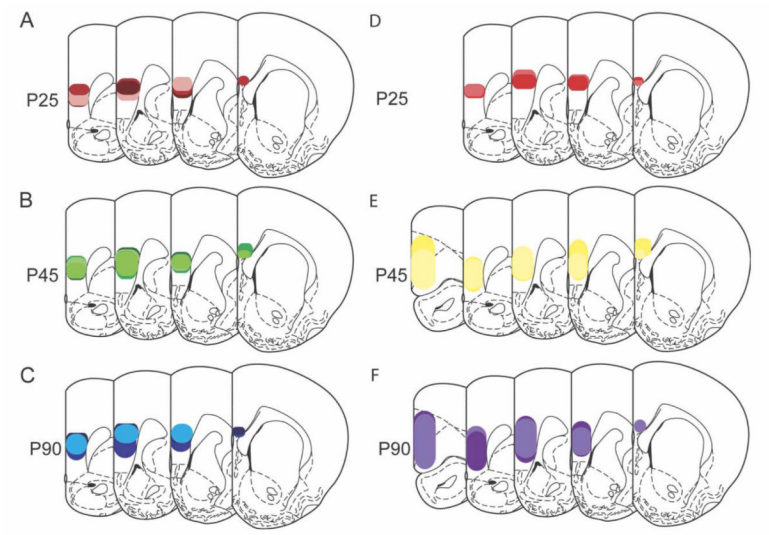

Figure 6.

Distributions of biotin dextran amine deposits within the mPFC. Biotin dextran amine was injected into the mPFC 6 days prior to collection of brains at P25, P45, or P90. Brains were selected for comparison based on their similarity of injection site and fell into two sets. In set 1 (**A–C**), all injection sites were located within a nearly identical region of the ventral PL and dorsal IL cortex. In set 2 (**D–F**), injections were centered in the ventral PL and matched very well in P45 and P90 brains but appeared to be somewhat more restricted in P25 brains. Individual injection sites are represented by different colors.

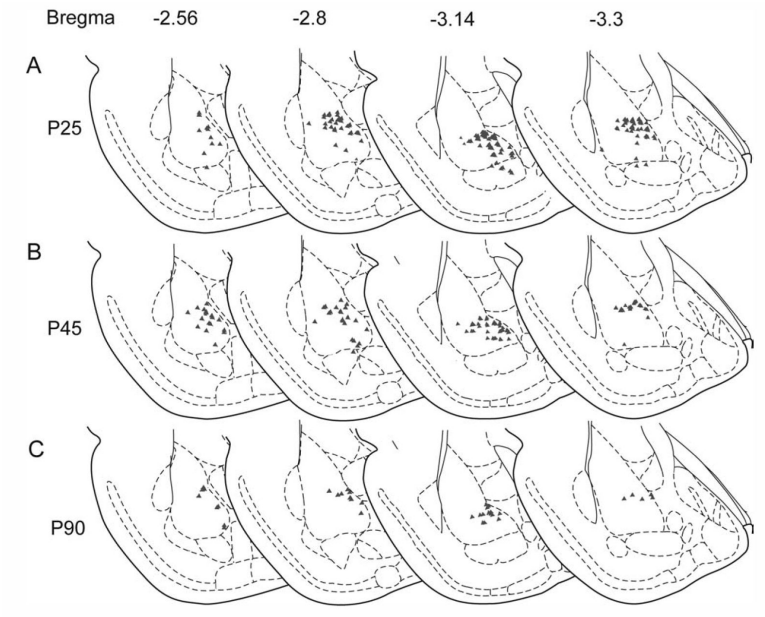

Figure 7.

Topographic distribution of anterogradely labeled fibers from the mPFC to the BA across adolescence and adulthood as detected with systematic random sampling. Examples are shown at P25, P45, and P90 of the distribution of BDA-labeled axon terminals in the BA following tracer injection into the ventral PL at sites shown in Figure 6. This representative distribution was determined using the L-cycloids optical fractionator method (see text). The sampling grid with 150 × 150 μm spacing was placed over the entire BA (regions included are shown in Fig. 1A). Symbols mark sites in the grid in which cycloid × axon intersections fell within the 70-μm counting frame.

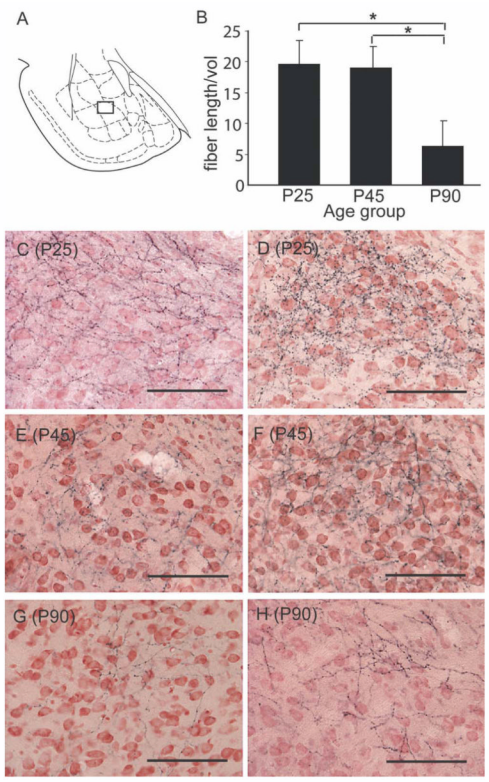

Figure 8.

Reduction in the density of mPFC axon terminals in the BA occurring between late adolescence and adulthood. **A**: Schematic diagram of amygdala; the boxed area encompasses the region represented in the photomicrographs C through G below. **B**: Density [mean ± SEM length (μm) per unit volume (μm^3)] of BDA-labeled terminals within the BA at P25, P45, and 90. *$P < 0.05$, P25, P45 > P90, planned pairwise comparisons. **C–H**: Representative photomicrographs from the dorsomedial region of the basolateral nucleus of two animals within each age group. The photomicrographs show black BDA-labeled fine terminal fibers with varicosities on a background of neutral red-stained cells (see Materials and Methods). Scale bars = 100 μm.

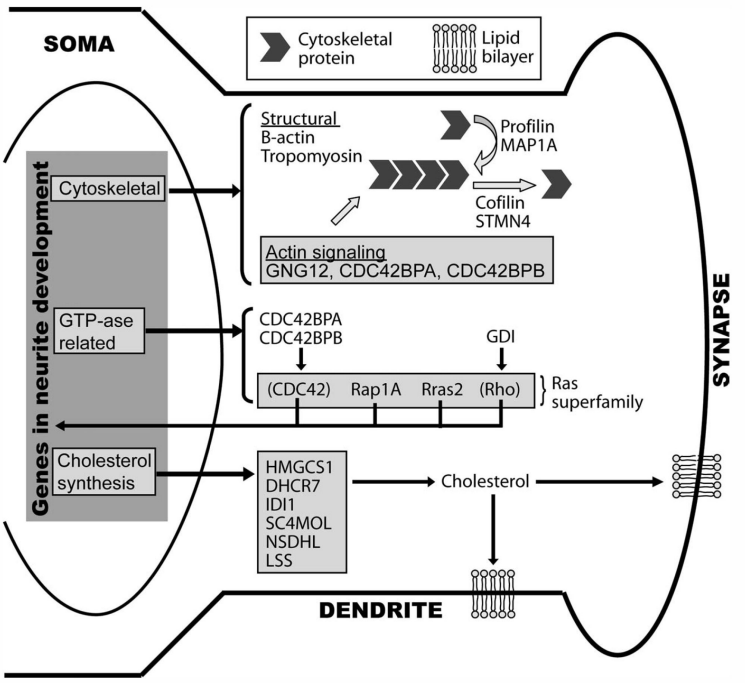

Figure 9.

Integrated view of changes in gene expression in the BA between late adolescence and adulthood. Potential biological functions of the products of genes differentially expressed at P45 and P90 are shown within the BA neuron. Genes coding for all proteins shown were differentially expressed with the exception of those in parentheses (CDC42 and Rho). The full name for abbreviated genes in the diagram can be found in Supporting Information Table 1. These proteins fall into three categories: those involved in the cytoskeleton (cytoskeletal), steroid/cholesterol biosynthesis (cholesterol synthesis), and Ras/GTPase pathways (GTP-ase related). Within the cytoskeletal group, structural proteins, such as actin, can polymerize via proteins, such as profilin and MAP1A, or depolymerize by using cofilin or STMN4. Other genes in the cytoskeletal cluster modulate actin signaling. The altered GTPase-related genes included members of the Ras superfamily, such as Rap1a and Rras2, and their regulators, such as CDC42BPA or GDI. The Ras superfamily pathways directly affect neurite dynamics as well as regulating transcription of proteins important in neurite dynamics. Finally, six genes directly involved in cholesterol synthesis may, via regulation of cholesterol levels, impact the extension/retraction of the lipid bilayer and/or insertion of cholesterol rafts at the synapse, which, in turn, affects anchoring of synapse-specific complexes.

TABLE 1

Stereotaxic Coordinates for Tracer Injections

	Basal amygdala			mPFC injection 1			mPFC injection 2		
	A/P	**M/L**	**D/L**	**A/P**	**M/L**	**D/L**	**A/P**	**M/L**	**D/L**
P25	−2.0	4.4-4.6	7.4-8.2	2.4-2.6	0.4	3.6-4.0	1.6-1.8	0.4	3.6-4.0
P45	−2.5 to −2.8	5.0	8.0-8.8	3.4-3.8	0.5	4.0-4.5	2.6-3.0	0.5	4.0-4.5
P90	−2.3 to −2.8	5.0-5.2	8.4-8.8	3.3-3.8	0.5-0.6	4.0-5.0	2.5-2.9	0.5-0.6	4.4-4.8

TABLE 2

Gene expression Differences Between P45 and P90 in the BA as Determined by ErmineJ

	Fold change[1]	*P* value
Cytoskeletal dynamics		
β-Actin	1.84	0.0000914
Endothelial differentiation sphingolipid G-protein-coupled receptor (S1pr1)	−1.85	0.00074
Tropomyosin 3 (TMP3)	−2.50	0.0011
Glia maturation factor beta (GMFB)	−1.92	0.0036
G-protein gamma-12 (GNG12)	−1.81	0.0075
Cofilin1	1.28	0.012
Stathmin-like 4 (STMN4)	−1.32	0.013
Microtubule-associated protein 1 A (MAP1A)	1.27	0.014
Profilin	1.41	0.015
CDC42 binding protein kinase beta (CDC42BPB)	1.28	0.017
CDC42 binding protein kinase alpha (CDC42BPA)	−1.32	0.02
Lipid metabolism and steroid-related processes		
Stearoyl-coenzyme A destaturase (SCD2)	−1.71	0.0012
3-Hydroxy-3-methylglutaryl-coenzyme A synthase 1 (HMGCS1)	−1.63	0.0012
7-Dehydrocholesterol reductase (DHCR7)	−1.31	0.012
Isopentenyl-diphosphate delta isomerase (IDI1)	−1.90	0.014
Sterol-C4-methyl oxidase-like (SC4MOL)	−1.39	0.014
NAD(P)-dependent steroid dehydrogenase-like (NSDHL)	−1.60	0.015
Lanosterol synthase (LSS)	−1.33	0.019
Ras/GTPase (12 genes)		
RAS-related protein 1a (Rap1a)	−1.47	0.013
Rho GDP dissociation inhibitor alpha (GDI)	1.21	0.012
Related RAS viral (r-ras) oncogene homolog 2 (Rras2)	−2.55	0.00022

[1]Positive -fold changes indicate P90 > P45.

J Comp Neurol. Author manuscript; available in PMC 2012 June 19.